International Journal of Mass Spectrometry xxx (2010) xxx–xxx

Contents lists available at ScienceDirect

International Journal of Mass Spectrometry

journal homepage: www.elsevier.com/locate/ijms

IMS–MS studies based on coupling a differential mobility analyzer (DMA) to commercial API–MS systems

Juan Rus[a], David Moro[a], Juan Antonio Sillero[a,b], Javier Royuela[a], Alejandro Casado[a], Francisco Estevez-Molinero[a,b], Juan Fernández de la Mora[b,*]

[a] SEADM, Parque Tecnológico de Boecillo, Valladolid, Spain
[b] Yale University, Mechanical Engineering Department, USA

ARTICLE INFO

Article history:
Received 6 December 2008
Received in revised form 17 February 2010
Accepted 5 May 2010
Available online xxx

Keywords:
Differential mobility analyzer
DMA
Cluster
Air
Tetrahexylammonium
Metastable
Charge loss
Electrospray

ABSTRACT

Recent progress in adding a mobility dimension to preexisting API–MS systems without modifying the MS itself is discussed, based on inserting a differential mobility analyzer (DMA) as part of the MS's atmospheric pressure ion source. Design criteria leading to high DMA resolving power R and transmission efficiency η are discussed. Various DMA prototypes have been interfaced to several triple quadrupoles, a single quadrupole and a quadrupole-TOF, all demonstrating $R > 50$ and $\eta > 50\%$. We obtain two-dimensional DMA–MS spectra of the multiply charged clusters formed in electrosprays of concentrated solutions of tetrahexylammonium bromide (A^+Br^-). These reveal systematic loss of $(ABr)A^+$ fragments from unstable multiply charged clusters, and provide mobility measurements in air on mass resolved $(ABr)_n(A^+)_z$ clusters with $n > 100$ and z up to 10. Well-defined bands of ions not individually resolved are clearly visible at considerably larger n and z values.

1. Introduction

Most ion mobility mass spectrometry (IMS–MS) work has relied on IMS systems separating pulsed ion packets in time. As shown in the present journal issue, this scheme has great analytical advantages, but has required the development of specialized hybrid instruments. For this reason, many commercial mass spectrometers still lack IMS capability, even though they are widely used and offer a level of reliability and sensitivity difficult to match by specialized developments. There is hence interest in the development of IMS systems suitable to be coupled to preexisting MS instruments, with as few modifications as possible to the MS itself.

Spatial mobility filters are devices separating a narrow range of ion mobilities *in space* rather than in time. Such instruments can yield a *steady* stream of mobility-selected ions, and can in principle be incorporated as part of the ion source of any preexisting atmospheric pressure ionization mass spectrometer (API–MS). Their practical interest became more widely appreciated with the development of FAIMS [1,2], a band pass filter of modest resolution that separates ions according to the nonlinear dependence of their mobility on the field strength. The only known *spatial* mobility filter capable of measuring true mobility with high transmission and resolving power in the range of 50–100 is the differential mobility analyzer (DMA) [3]. Here we describe the design and capabilities of the first DMAs of high resolving power (>50) and high transmission (~50%) having already been coupled to several commercial API–MS systems. We then use a DMA coupled to a TOF-MS of high resolution and wide mass range to study the complex spectrum of large multiply charged clusters produced by electrospraying concentrated salt solutions.

2. The DMA and DMA–MS design considerations

Devices combining fluid flow and electric fields for separating charged particles in space according to their electrical mobility have been used for a long time [4], with many variants described by Tammet [5] and Flagan [6]. Early attempts to use such systems in ion mobility separation proved unsatisfactory, primarily due to diffusive broadening of the ion beam perpendicularly to its direction of propagation. Diffusion limits the resolving power to values of the order of $(U\Delta/D)^{-1/2}$, where U (cm/s) is the flow velocity, Δ (cm) a characteristic length and D (cm^2/s) the ion diffusivity in the

* Corresponding author at: Department of Mechanical Engineering, Yale University, PO Box 208286, 9 Hillhouse Avenue, New Haven, CT 06520-8286, USA. Tel.: +1 203 4324347; fax: +1 203 4327654.
E-mail address: juan.delamora@yale.edu (J. Fernández de la Mora).

1387-3806/$ – see front matter © 2010 Elsevier B.V. All rights reserved.
doi:10.1016/j.ijms.2010.05.008

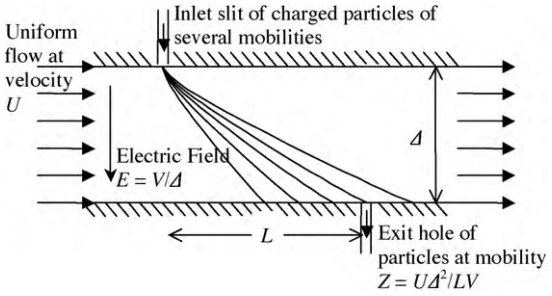

Fig. 1. Sketch of a planar DMA where ions are injected from the top through an inlet slit into a flow field U between two parallel electrodes separated by a distance Δ. An electric field E (V/cm) pushes the ions downwards at velocity ZE as the flow U carries them to the right, so that the trajectories separate into a fan with a slope proportional to the electrical mobility Z. Ions with a selected mobility Z are sampled into a mass spectrometer through a small outlet on the bottom plate.

bath gas. We shall from now on restrict the discussion to the most common spatial mobility filter, the so-called differential mobility analyzer (DMA), illustrated in Fig. 1 for the simplest parallel electrode geometry. In this device, the diffusion-limited relative full width at half maximum (FWHM; dimensionless quantity) for an ion of narrowly defined diffusivity D cannot be less than (1) [7]:

$$\mathrm{FWHM}^2 = 32 \ln 2 \frac{D}{U\Delta}. \quad (1)$$

The measurement of FWHM is performed as follows. Ions of fixed mobility Z ($\mathrm{cm^2\,V^{-1}\,s^{-1}}$) are injected continuously at the inlet slit. The DMA is run at constant gas velocity U, and the voltage difference V (V) applied between the two electrodes is varied continuously from zero to a maximum value. Then, the curve $I(V)$ representing the ion signal I (nA) recorded at the outlet slit as a function of V is zero everywhere except for a *peak* appearing at a narrow range of values of V. FWHM is defined based on the FWHM of this $I(V)$ peak, normalized by the mean voltage V_o at the center of the peak. The ion mobility Z is in turn strictly proportional to the inverse of the peak DMA voltage: $Z \sim 1/V_o$, where V plays very much the same role as the time in drift tubes. Hence, $\mathrm{FWHM}_V = \mathrm{FWHM}_Z$.

Eq. (1) shows that $U\Delta/D$ must exceed 2.2×10^5 for the resolving power (1/FWHM) to become 100. Achieving this rather high value is complicated because the diffusivity D of small ions is comparable to the kinematic viscosity ν ($\mathrm{cm^2/s}$) of the carrier gas; $D/\nu \sim 1$. Therefore, for $U\Delta/D$ to be large, the Reynolds number

$$\text{Reynolds number} = \frac{U\Delta}{\nu} \quad (2)$$

must also reach very high values, which tends to generate turbulence in the fluid, and limits resolution even more drastically than diffusion. This difficulty does not exist in drift tube IMS, where fluid velocities are negligible compared to ion drift velocities. As a result, DMAs have been used primarily for the separation of relatively large charged particles, for which D/ν is small [8], and good resolution can be obtained at moderate Reynolds numbers. Although the DMA concept is very old [6], its wide use in aerosol studies originates in the instrument developed by Knutson and Whitby [9], which was commercialized by TSI (St. Paul, MN).

Efforts to develop DMAs able to operate at high (supercritical) Reynolds numbers began in the nineties [10], facilitated by the availability of electrospray sources of atmospheric pressure ions with sharply defined mobility [11]. The viability of supercritical flows rests on the fact that transition to turbulence takes a finite time, which can be greatly increased in situations initially highly laminar. As in conventional wind tunnels, a much reduced level of time-dependent velocity fluctuations is achieved by passing the flow through several *laminarization* screens followed by a substantial acceleration through a converging section (Figs. 2 and 3). As long as mobility separation is completed before turbulent transition takes place, resolving powers in excess of 100 are achievable, in theory [7,12], and in practice [3]. Several examples of the power of the DMA–MS combination have been available for some time [13,14], though based on conventional cylindrical DMAs in which ion transmission from the ES source into the separation section of the DMA is poor.

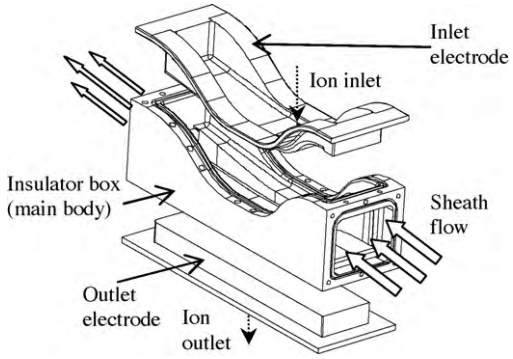

Fig. 2. Schematic of a rigid and leak-tight DMA based on an insulating box (middle) with inlet and outlet openings for the high speed gas flow (right and left, respectively), and top and bottom openings to support the inlet and outlet electrodes, respectively. Note a large inlet laminarization trumpet (right) with support for several laminarization screens, and a slowly diverging outlet section or *diffuser* to the left.

2.1. Planar DMAs

The potential of a parallel plate geometry to achieve high ion transmission in ES-DMA–MS has long been recognized [15]. But the development of a practical DMA–MS coupling has been slow due to several technical difficulties. A first *geometrical* problem is the need to arrange a pair of opposite conducting surfaces separated by insulating surfaces in a fashion avoiding gas leakage, and offering very smooth surfaces to the flow, so as to avoid turbulence transition at the high Reynolds numbers required for successful operation. Initial studies [16,17] achieved the desired matching between the insulator and the conducting electrodes by constructing the electrodes out of thin metal sheet pieces supported by a system of thicker plates and screws on both sides of an insulating structure. But, due to a variety of difficulties, this configuration could not be run at the high speeds required to attain very high Reynolds numbers. First due to gas leakage and associated formation of destabiliz-

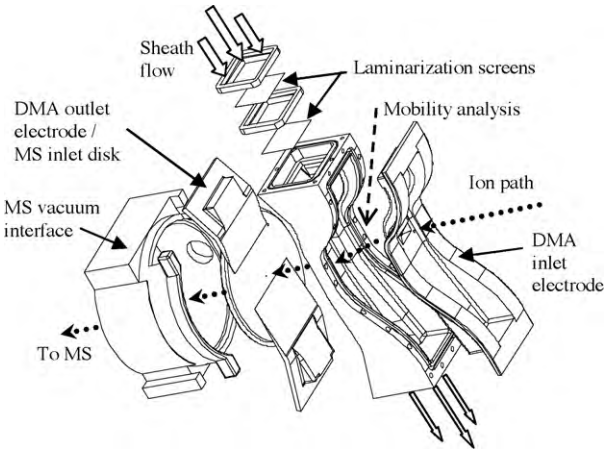

Fig. 3. Details of the direct coupling of a flat DMA to the vacuum interface of a mass spectrometer (left). The standard disk piece holding the orifice sampling gas into the MS vacuum is extended and turned into the lower plate of the DMA.

Please cite this article in press as: J. Rus, et al., Int. J. Mass Spectrom. (2010), doi:10.1016/j.ijms.2010.05.008

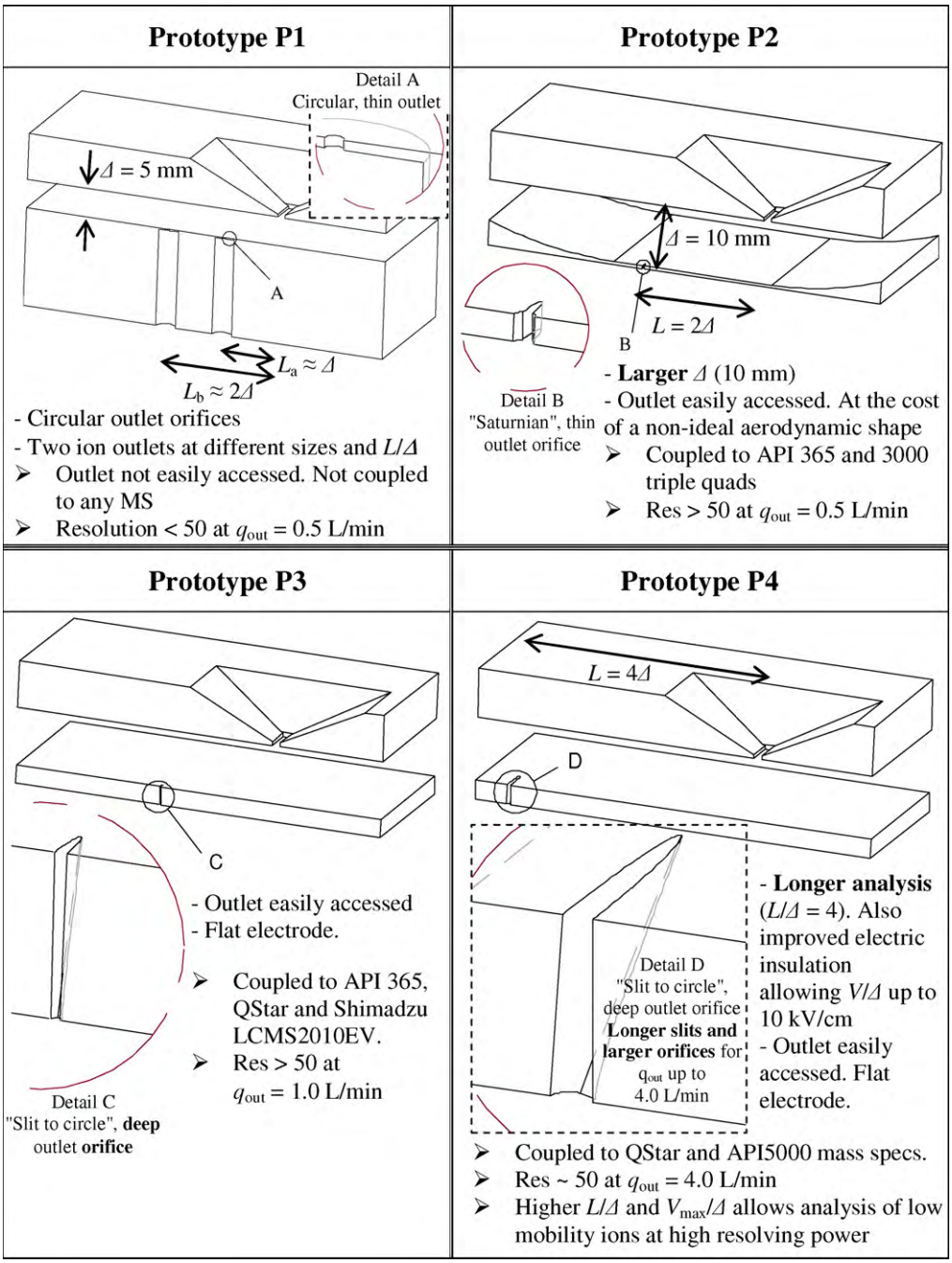

Plate 1. Sketches of various features marking the evolution of parallel plate DMA prototypes and their coupling to the MS (Longitudinal section).

ing jets in the analyzing region. Second because small steps could not be avoided at points where the material forming the flow surface changed from a metal to an insulator. Third, because the DMA electrodes were made out of thin metal sheet, which, due to considerable pressure differences between their inner and outer surfaces, deformed at the desired high gas speeds. Note in this respect that near-sonic speeds are most desirable to achieve high Reynolds numbers, and these require a pressure close to two atmospheres at the laminarization structure when the analyzing region is at atmospheric pressure. A variation in Δ by 1% across the length of the slit leads to an increase of 1% in FWHM. Attaining near-sonic speeds with pumps of practical dimensions calls also for a long diffuser at the exit of the instrument, where the high velocity is converted into pressure to reduce drastically the pump power required to drive the gas flow [18]. In spite of these difficulties, the DMA was tested at moderate speeds, at which leaks and plate deformation levels were tolerable, demonstrating high transmission [16,17]. But the best resolving power reached was ~50, and more typically 30 in day-to-day operation, considerably worse than the values previously demonstrated for a DMA alone.

Given this experience, the present designs have been generically based on rigid insulating structures such as that shown in Fig. 2, where a leak-tight operation is assured by sealing o-rings in all four openings.

2.1.1. *Matching the linear DMA outlet slit to the round MS sample inlet orifice*

Some of the initially unclear causes for the limited resolution previously achieved in flat DMA–MS coupling have to do with the change of symmetry from the planar DMA to the cylindrical MS

inlet [19]. In the early designs (P1 in Plate 1), the exit slit of the DMA coincided with the sampling hole of the MS, both being part of the same circular orifice drilled in the lower electrode. In this arrangement, as shown in Appendix A, the DMA resolution can be at most of the order of $(Q/q)^{1/2}$, where Q is the gas flow rate through the DMA and q is the gas flow rate sampled into the MS through the orifice, typically 0.5 L/min or more. In contrast, the resolution of a conventional cylindrical DMA with a circular sampling slit, or that of a planar DMA with a linear sampling slit scales ideally as Q/q [9], which is much larger than $(Q/q)^{1/2}$ when Q/q is large. In spite of these difficulties, Rus et al. [20] reported excellent resolving power (60–80) for a planar DMA coupled to several mass spectrometers, including the API 365 triple quadrupole and the q-TOF (Q-Star), both from Sciex, and both sampling 0.5 L/min. However, this performance required limiting the sample flow rate at the DMA outlet (coinciding with the MS inlet) to about 0.3 L/min with a round orifice of 0.18 mm, which impaired the ion transmission in both mass spectrometers.

The $(Q/q)^{1/2}$ resolution limitation noted has been addressed and resolved by two different schemes, all partly preserving the planar symmetry of the DMA at its outlet, turned now on the DMA side into an elongated orifice [19]. In one instance the plate separating the DMA from the vacuum system of the MS was perforated all the way with a slit-shaped orifice, so that an elongated rather than a round supersonic free jet formed on the MS side (P2 in Plate 1). This approach permits good ion transmission in the MS, though with some required modifications in the skimmer positions and RF voltage in the ion guides once the slit elongation exceeds a certain threshold. Excellent resolution (>50) and ion transmission (>50%) has been reported for this configuration, implemented in Sciex's API 3000 triple quadrupole [21]. Particularly noteworthy in this study is the drastic increase in signal/noise provided by the DMA when spiking very small concentrations of analyte in complex matrices such as urine. This report used liquid chromatography (LC) upstream of the DMA–MS, and shows instances where the tandem DMA–MS sees only one peak in an otherwise crowded chromatogram. In certain circumstances, therefore, the LC may be substituted by the much faster DMA (10^{-4} s).

A related approach successfully tested that eliminates the need for modifications on the MS end and allows MS sample flow rates considerably larger than 0.5 L/min simply uses a shaped conduit changing from a slit-shaped DMA exit orifice into a round MS entry hole (P3 and P4 in Plate 1). In order to avoid affecting the nominal MS sample flow, the slit end has a wider cross-section than the circular end, so that the flow becomes critical only on the latter. This system has been implemented on Sciex's Q-Star (Section 3) and API 365 instruments, on DMA prototypes where the thickness of the lower electrode piece is sufficient to accommodate the slit-circle transition. A similar solution has been used in Shimadzu's LCMS-2010EV single quadrupole MS, whose inlet capillary is readily coupled via a standard chromatography adaptor to the slit-circle shaped sample outlet on the lower electrode of the DMA [22].

2.1.2. Mechanical coupling between DMA and MS

The details of the mechanical coupling between the two instruments have varied depending on the characteristics of the MS. In the three Sciex instruments used (API 365, API 3000 and Q-Star), the MS inlet hole is located in a flat disk, which has been used as the lower electrode of the DMA with appropriate elongations to include the DMA main flow inlet and outlet sections, as sketched in Fig. 3. The figure shows also the vacuum interface piece of the MS, cut on two sides to accommodate the extended lower electrode. The flow surface of this electrode includes two bends, to accommodate the DMA flow channel without thickening the disk (P2 in Plate 1). Other prototypes with a thicker plate and a flat lower DMA electrode have been similarly successful (P3 and P4 in Plate 1). Fig. 3 shows details on the placement of the laminarization screens (top) and the ion inlet for the DMA (right; see also Fig. 2). The slit has a much smaller depth than the rest of the plate in order to allow penetration of the internal and external electric fields. As a result, the ions produced right outside of the slit can be driven through it by these fields against a flow of dry gas exiting the slit from inside to outside the DMA. This counterflow plays the same drying and cleaning role as the curtain gas used in various API mass spectrometers. It is further required here in order to avoid solvation of small ions in the DMA by humid ambient air. This would disperse their signal over different solvation states, complicating the spectrum and spreading the ion signal over many mobilities.

2.1.3. Flow circuit and other design features

The DMA flow rate associated to the flow field U achieving ion separation (termed the *clean* or *sheath* gas) is typically above 1000 L/min in a DMA geometry with electrode separation $\Delta = 1$ cm (with a flow section in the separation region of 1–2 cm^2). Because it is impractical to dry such large quantities of atmospheric air, the sheath gas flow is recirculated from the DMA outlet to its inlet through a relatively clean and leak-tight vacuum pump. The pump consumes a power approaching 1 kW, which heats up substantially the recirculating gas. Closing the circuit with flexible corrugated metallic lines provides sufficient heat transfer to the atmosphere to keep the gas flow below 30–40 °C up to a flow Mach number $M \sim 0.5$. Dry clean gas is injected into the sheath gas circuit, in order to replace the gas sampled by the MS and the counterflow drying gas leaving through the DMA inlet slit. After a short initial period, this clean gas purges all the humid gas initially in the closed circuit.

3. Description and performance of various DMA generations

We summarize here several years of experience obtained with four DMA prototypes, whose main characteristics are collected in Table 1 and illustrated in Plate 1.

P1. It was built to test the new box structure, with an electrometer detector in lieu of a MS. Sonic conditions were achieved with a vacuum cleaner pump, at ~600 L/min (Reynolds number of 0.97×10^5), with laminar flow. The resolving power was below 50 at the desired sample outlet flow (0.5 L/min).

Given the resolution limitation, the gap was doubled in subsequent prototypes ($\Delta = 1$ cm; Reynolds number approaching 1.90×10^5). This complicates reaching sonic conditions, but Mach numbers near 0.8 are achieved, still with laminar flow.

P2. Δ was doubled to 1 cm. The entrance and exit regions were not widened comparably, leading to much reduced area ratios of the

Table 1
Geometrical characteristics of the various DMAs tested.

DMA	L (cm)	Δ (cm)	Sample outlet shape	Length/width outlet shape (mm)	Length/width inlet slit (mm)
P1	1 and 2	0.5	Various round orifices	Several tests Ø0.10–0.25	5/0.3 and 5/0.1
P2	2	1	Slit (*Saturnian* shape)	0.5/0.10	~10/0.3
P3	2	1	Slit and slit-hole	0.45/0.22 and 1.5/0.15	9/0.3 and 17/0.6
P4	4	1	Slit-hole	0.6/0.15	4/0.6 and 17/0.6

Please cite this article in press as: J. Rus, et al., Int. J. Mass Spectrom. (2010), doi:10.1016/j.ijms.2010.05.008

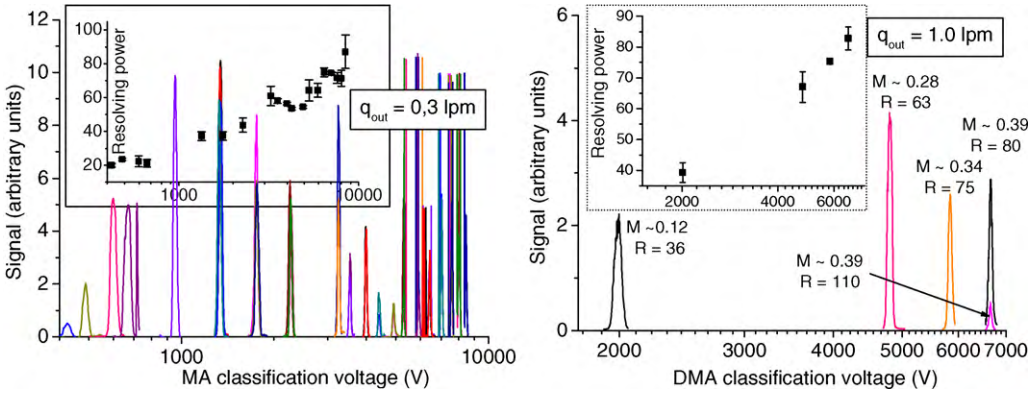

Fig. 4. Performance of the P3 models. Left, circular 180 μm outlet orifice on DMA and MS sides. Right, shaped slit-round outlet slit at much increased sample flow.

convergence and the diffuser (from 30 to 9 and from 6 to 4, respectively). Resolving powers >50 were achieved. The DMA was simply installed in Sciex's API365 triple quad at Yale (Fig. 3). It initially sampled 0.3 L/min through a round orifice, later widened laterally into a Saturnian shape sampling 0.5 L/min. Excellent performance was achieved when coupled to Sciex's API 3000 triple quadrupole [21], though the elongated orifice and associated rectangular free jet required modifications within the MS.

P3. In this and subsequent models, the channel communicating the DMA outlet to the MS inlet became longer to accommodate a shape transition from a slit to a round hole (fabricated via wire-EDM). The thicker DMA outlet plate also permits a completely flat lower electrode. The resolution exceeded 50 up to sampling flow rates of 1.8 L/min, enabling coupling the DMA to Shimadzu's LCMS-2010EV single quadrupole MS sampling 1 L/min. Fig. 4 shows the performance of the first P3 model at two different configurations: with a round outlet orifice similar to P2 (left) and with the enlarged orifice with a transition from a slit to a round hole (right). We have in fact reached 100 resolving power in this last prototype (with a long DMA outlet slit, 1.5 mm long, 0.15 mm wide), although at the cost of decreasing the inlet flow of ions and the transmitted signal (see the small, high-resolution peak at 6650 V in Fig. 4 right). Note, however, that these DMAs operate at vast Reynolds numbers, and transition to turbulence is sometimes detected under certain operational conditions.

P4. This model, used for the studies of Section 4, was the first commercial planar DMA product readily coupled to several commercial mass spectrometers. Its longer $L/\Delta = 4$ expands widely the instrument's ability to select low mobility ions.

3.1. Ion transmission

Ion beam spreading inside the DMA due to diffusion or other broadening effects has two different kinds of consequences. For a given exit slit, a narrower ion beam transmits more efficiently ions with the selected mobility (high transmission), while admitting a narrower range of ions with neighboring mobilities (higher resolution). Hence, high resolution and high ion transmission are almost synonymous for all parallel plate DMAs. This appears to be the opposite of what happens in conventional IMS, where high resolution calls for long flight paths, hence poor transmission (unless the ions are confined by special means). However, this advantage of the DMA over drift IMS is really incidental, since the two suffer the same Brownian broadening process, governed in IMS by $Vze/(kT)$ (ze is the charge on the ion, e is the elementary charge), which is identical to $U\Delta/D$ when using the drift velocity ZE in lieu of U. The real difference follows from the limited field E attainable when IMS is practiced at low pressures and with noble drift gases, which calls for drift distances much larger in pulsed systems than in DMAs. While much shorter drift distances could be used in pulsed IMS in atmospheric air, the resulting unusually short drift times (100 μs) would have to be measured with ~1 μs resolution.

Several measurements of DMA transmission have been made, confirming generally the theoretical notion that it tends to be high when the resolving power is high. For instance, Javaheri et al. [21] have compared the ion signal obtained in their triple quadrupole MS when either putting the DMA (P2 in Table 1 and Plate 1) or not. They report comparable ion fluxes to the MS, implying ion transmission efficiencies above 50%. We have complemented these DMA–MS transmission studies with two kinds of measurements on the DMA alone. In one, with all other conditions fixed (including ion concentration n at the DMA inlet slit), the resolution and ion current I passed through the outlet orifice were measured as a function of sample outlet flow q (Fig. 5 left). The ion transmission curve exhibits a plateau above 1 L/min, and a region of low sample flow rates where the current I is approximately linear with q, $I \sim q$. The plateau can be interpreted as a high transmission condition when most ions entering the DMA are passed to the MS. Further increases in q (beyond the value of $q \sim 1$ L/min achieving this high transmission) have only minor effects on the ion current, since the additional outlet gas sampled is clean gas. In other words, in the plateau region, the average ion outlet concentration $\sim I/q$ decreases with q because the ion beam entering the DMA is narrower than that sampled out of the DMA, whereby the sample outlet is diluted with clean air. There is no point in operating at sample outlet flows higher than 1 L/min because the resolution decreases with no transmission advantage. The approximately linear region at $q < 1$ L/min implies that the ion concentration n at the outlet slit is nearly fixed, since the ion current I is $I = nzeq$ in the absence of losses on the outlet line. This shows that there is no dilution associated to beam broadening, with an ion beam broadening effect as irrelevant as in the plateau region. These data then show indirectly that the ion transmission is excellent down at least to $q = 0.5$ L/min. The well known optimal condition of operation (where transmission is high without impairing resolution) is at the corner where the linear region meets the plateau [9].

We have quantified transmission more directly by fixing the ion density n_1 just upstream of the DMA inlet with a new tandem DMA–DMA technique [23]. A first DMA is operated with recirculating sheath flow using electrospray-generated tetraheptylammonium$^+$ ions (THA$^+$), with DMA flow rate and voltage fixed such that its sample outlet carries only THA$^+$ ions as verified by initially taking a full mobility spectrum at fixed flow rate and variable voltage, and comparing it with the published DMA–MS spectra [24]. This provides a steady stream of ions of sharply defined mobility at a fixed concentration n_1, whose magnitude we determine by measuring the outlet flow q_1 and the total current I_1 it carries: $n_1 = I_1/(eq_1)$. The current I_1 is measured by an amplifier con-

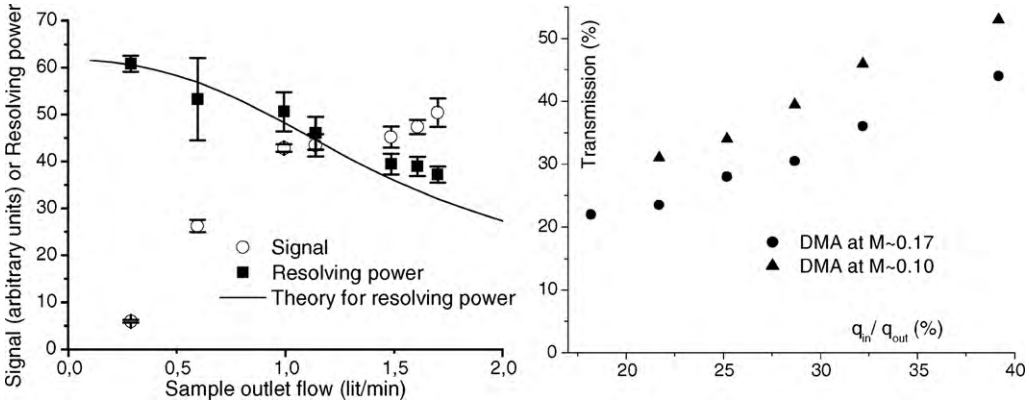

Fig. 5. Dependence of DMA transmission on sample flow for tetraheptylammonium$^+$ ions. Left, P3 DMA with fixed ion concentration at the sample inlet and variable outlet flow. Right P4 DMA with upstream ion concentration fixed via tandem DMA operation, while operating at a variable inlet flow rate (suction).

nected to an enclosed metallic filter, where the ions are captured as the gas carrying them passes through the filter. In order to correct for ion losses to the tubing walls, the line carrying the ions has two segments with identical length (and losses), one leading to the vicinity of the sample inlet slit of the second DMA, and the other leading to a filter connected to the current amplifier. This arrangement provides a jet of air carrying ions at a known concentration n_1, with which we bathe the inlet slit of the *test* DMA whose transmission we wish to evaluate. In this case, the *test* DMA (P4 in Table 1) is operated at a fixed velocity (Mach number ~0.10 or 0.17), sample outlet flow rate q_{out} = 0.8 L/min, and a varying inlet flow rate q_{in}. We use sample suction rather than counterflow gas, because of the difficulty to control the electric field needed to push the ions against the counterflow stream of gas in the presence of the large 1/4″ OD diameter of the tube bringing the calibration ions in. However, the situation with counterflow gas would theoretically be quite similar, as long as the driving field E produces ion drift velocities several times larger than the opposing counterflow gas velocity. The voltage of the test DMA is ramped around the value associated to THA$^+$, from which peak width and height are inferred. These experiments were carried out at limited DMA voltages, with modest resolutions of about 40. Ion transmission is defined as the ratio between the ion concentrations at the outlet and the inlet of the test DMA, both given by $I/(qe)$. The outlet current of the test DMA was measured similarly as in normal operating conditions, by pumping on the chamber immediately downstream from the DMA outlet orifice, and placing a collector electrode a few mm downstream. In order to be sure that the collector captured all the ion current carried by the supersonic free jet of sample expanding from the DMA outlet into the low pressure chamber, the voltage difference established between the lower DMA electrode and this collector was increased until no further increase in collected current resulted. The transmissions measured are shown in Fig. 5 (right) as a function of the outlet to inlet sample flow rate ratio per unit slit length. The advantage of this representation is that, ideally, the response would be $y = x$ for $x < 1$, $y = 1$ for $x > 1$, as argued in the discussion of Fig. 5 (left). This expectation is in fact met approximately, confirming quantitatively the earlier independent conclusions that ion transmission efficiencies are excellent.

4. Multiply charged clusters from electrosprays of concentrated electrolytes of tetrahexylammonium bromide

We have tested the analytical characteristics of the P4 DMA coupled to Sciex q-Star quadrupole-TOF by analyzing the complex mix of ions produced by electrospraying a concentrated alcohol solution of tetrahexylammonium bromide (ABr). This spray produces multiply charged clusters of the form $(ABr)_n(A^+)_z$, with two-dimensional complexity associated to the levels n and z of clustering and charge, respectively. Multiply charged ES clusters have been studied since the pioneering work of Meng and Fenn [25], which reported (n, z) values as large as (24, 4) for arginine clusters. The ability of arginine or other aminoacids to form clusters holding multiple charges is outstanding. For instance, Myung et al. [26] have investigated proline clusters by IMS–MS, and see up to 7 charges at m/z = 2300 Da ($n \sim 140$). In the case of salts, few such studies have reported charge states beyond z = 2. Exceptionally, the ion components of the large organic salt tetraheptyalmmonium bromide bind to each other strongly enough to form large and highly charged clusters [13]. These aggregates have been studied previously with DMA–MS, though with low transmission efficiency in the DMA. This yielded good mass spectra, but only after 10–60 min of signal accumulation at each mobility, precluding acquisition of full DMA–MS data. The use of the low vapor pressure solvent formamide allowed using very high salt concentrations [13], precluded here by solute precipitation on the emitter due to the higher volatility of the alcohols used (methanol and ethanol). But the formamide solutions produced mixed clusters of NH_4^+ and tetraheptylammonium$^+$ complicating considerably the spectra and their interpretation. In contrast, the present alcohol solvent (or perhaps the greater purity of the salt) produces mass spectra containing almost exclusively $(ABr)_n(A^+)_z$ peaks.

4.1. Experimental

The inlet slit to the DMA has a width of 0.6 mm. An electrospray chamber was fitted to it so that the electrospraying silica capillary (50 μm ID, 360 μm OD sharpened conically down to the ID; Polymicro Technologies, Phoenix, AZ) was well centered with respect to the slit. The capillary could be moved along the needle axis, to approach the slit as much as desired, and even penetrate through it. The Taylor cone could be observed through a pair of opposite windows on the ES chamber, but only when its distance to the slit exceeded ~2 cm. The Taylor cone was controlled by fixing the pressure ΔP pushing the liquid through the capillary from a pressurized reservoir into the emitting tip, increasing the voltage until a stable Taylor cone formed. At fixed ΔP, we then measured the range of associated ES current I_{ES} at which the Taylor cone (monitored visually) was stable upon varying the voltage. The needle was then slowly moved away from the field of view towards the inlet slit of the DMA, while continuously adjusting the ES voltage such that the current remained close to a preset value, always within the stable range. Once fixed at an axial position yielding a good MS signal and a stable ES current, we proceeded to acquire the DMA–MS spectrum

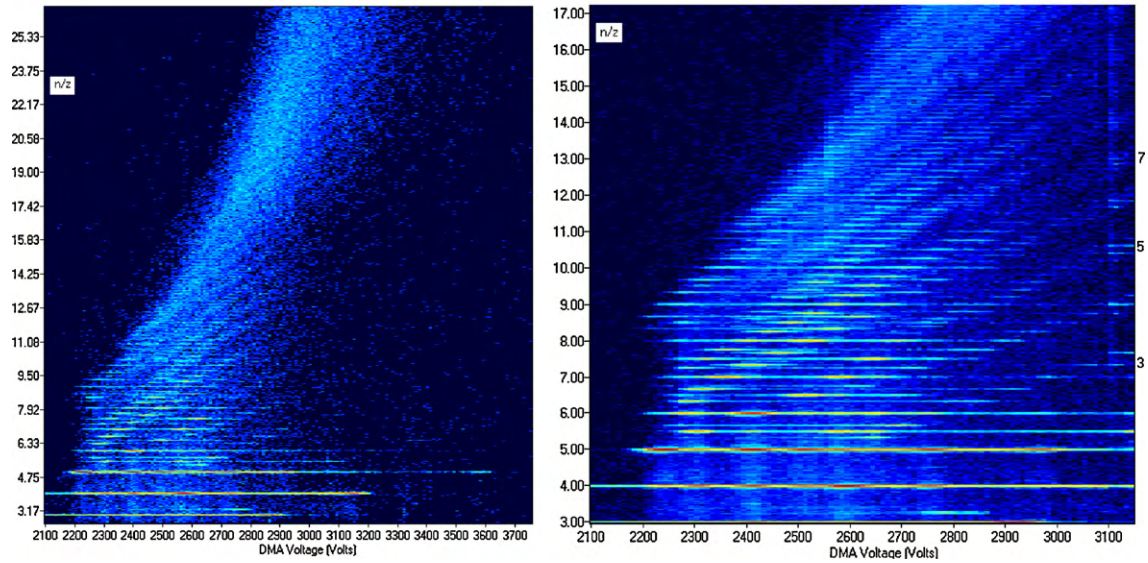

Fig. 6. DMA–MS spectra for an electrospray of a concentrated methanol solution of tetrahexylammonium bromide. The DMA voltage is proportional to the inverse mobility [Eq. (4)]. The vertical scale is n/z. Left: full spectrum up to 12,000 Da. Right, detail at intermediate masses showing more clearly the diagonal bands associated to individual charge states.

while occasionally monitoring the ES current for long-term stability. The distance from the tip of the needle to the inlet slit could not be measured precisely, but it was in the range of 100 μm. The organic salt was dissolved in methanol at 20 mM, producing a fairly conducting solution whose minuscule drops evaporated efficiently in the short distance available, against a counterflow of air typically between 0.3 and 0.5 L/min (mean flow speed of 2.5–3.5 m/s). The DMA operated in closed circuit, with a gas flow driven by a vacuum cleaner pump. Clean bottled air was introduced at a controllable flow rate at a certain point in the circuit. Because the circuit, the DMA and the pump are leak tight, this gas had to leave the system partly as sample to the MS, with the balance departing as counterflow gas. This flow was measured with a flowmeter as it left the chamber into the atmosphere through an outlet tube.

The q-Star was operated under conditions such as to minimize ion fragmentation downstream of the DMA. In particular, the focusing and declustering potentials were set to 1 V (DP = FP = DP2 = 1 V; IRD = 6 V; IRW = 5 V). The software controls simultaneously the DMA and the MS, executing sequentially the acquisition of mass spectra for a certain preprogrammed period at a set of DMA voltages. These two-dimensional DMA–MS data are then stored as single files.

4.2. Results

Fig. 6 shows two DMA–MS spectra for electrosprays of a concentrated tetrahexylammonium bromide solution (total acquisition times of 8 and 51 min, in the left and right images, respectively). For simplicity we will refer to $(ABr)_n(A^+)_z$ species as n^z, while the vertical scale is in terms of n/z rather than m/z:

$$n/z = \frac{(m/z - 354.66)}{434.6} (m/z \text{ in Da}).$$

The representation is based on SEADM software incorporating a logarithmic color scale covering a range of up to six orders of magnitude of signal intensity, and allowing averaging in the m/z coordinate from zero up to 30 Da. Most intense contributions arise at the horizontal lines for singly charged clusters at $n/z = 3$–6. Visible also are the doubly and triply charged series, unambiguously present already at $n/z = 5 + (1/2)$ and $5 + (2/3)$, respectively. There are almost no impurity peaks in the mass spectra, so that many other series can be identified. The assignment of masses to each mobility peak is complicated by the instability of many ions, which leads to transitions of the type:

$$n^z \rightarrow (n-p)^{z-1} + p^1; \quad p = 0, 1, \ldots \tag{3a}$$

If these transitions took place inside the DMA, one would see a mobility intermediate between the precursor and the product, with all intermediate mobilities being represented in a broad peak, depending on where in the DMA the transition happened. Therefore, the narrow mobility peaks observed indicates that most of these transitions occur downstream from the DMA. Accordingly, the mobility and m/z measured are for the parent and the daughter ions, respectively. As a result, each cluster mobility leads to several m/z peaks, each associated to a different transition of the precursor ion (including no transition). Similarly, each mass exhibits several mobility peaks, a point more obvious in Fig. 6 due to the much higher resolution of the MS ($\sim 10^4$) than the DMA (~ 60). This multiplicity of mobility peaks is especially clear in Fig. 6 at $n/z = 3$–5. One can see in Fig. 6 (right) also two continuous series of apparently doubly charged mobility peaks (spaced by half units in n/z coordinates) staring at $n/z = 5 + (1/2)$. Also two clear $z = 3$ series, one on the far right labeled 3 and originating at $n/z = 5 + (1/3)$, another starting on the left, and originating at $n/z = 5 + (2/3)$.

4.3. Singly charged ions

Fig. 7a shows a DMA–MS spectrum of the lower mass region going up to 2962 Da ($n/z = 6$), showing (with minor exceptions) only singly charged mass peaks. Relevant DMA–MS information can therefore be summarized as the six mass-selected mobility spectra shown in Fig. 7b for the masses of clusters $(ABr)_nA^+(n^1)$ with $5 \geq n \geq 0$. Only one mass peak arises at the highest mobility (1250 V, $n = 0$), which can be unambiguously associated to the monomer ion A^+. Its electrical mobility in air Z_o has not been measured precisely. But under the same DMA velocity we see the dimer ion of tetraheptylammonium ($Z = 0.654\,\text{cm}^2\,\text{V}^{-1}\,\text{s}^{-1}$ according to Ref. [24]) at 2100 V, leading to $Z_o = 1.1\,\text{cm}^2\,\text{V}^{-1}\,\text{s}^{-1}$ (±2%). Accordingly the mobility in ambient air for an ion appearing at voltage V_{DMA} can be inferred as:

$$\frac{Z}{Z_o} = 1250/V_{DMA}\,(V_{DMA} \text{ in Volt}). \tag{4}$$

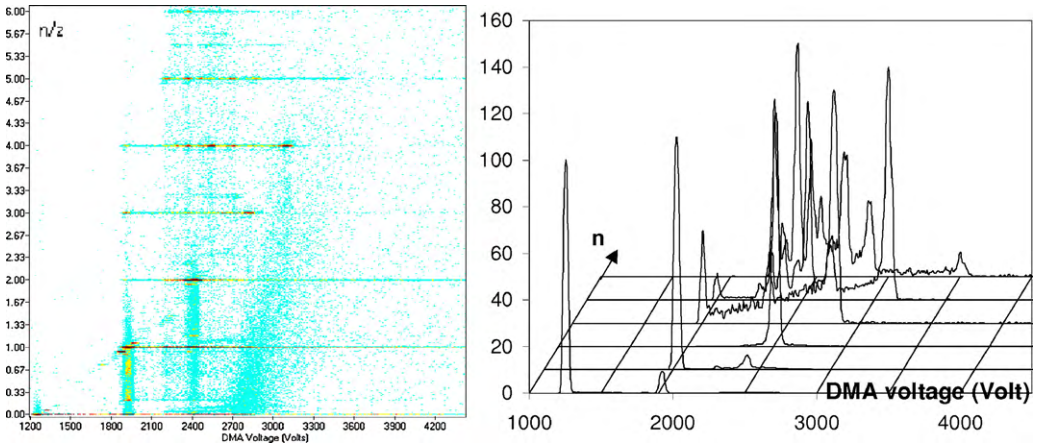

Fig. 7. DMA–MS spectra in the region of singly charged clusters $(ABr)_nA^+(n^1)$ with $0 < n < 5$. Note a fuzzy band of impurity peaks, starting with 0^1 on the lower left, and joining the various n^1 clusters. The right pane shows the six mass-selected mobility spectra (normalized to 100) associated to the masses of n^1 clusters.

A single mobility peak arises at the mass of the trimer ion 2^1, making its mobility assignment unambiguous. The mobility of the dimer ion 1^1 is also unambiguous, since the corresponding mass shows only one dominant peak with a mobility intermediate between those of the monomer and the trimer. Mobility assignment is less obvious at the masses of 3^1, 4^1 and 5^1 ions, all exhibiting several sharp mobility peaks, as well as regions with a continuous mobility distribution. However, most of these mobility peaks are repeated at several of the singly charged cluster masses, and can be seen to be decomposition products of multiply charged ions. This is clear in Fig. 7 for the mobility peak at 2400 V. By excluding such peaks and requiring a continuous dependence of the peak voltage on n, one arrives at the assignment shown in Table 2, where the correct peak at each of the masses is the tallest one, except in the case of 5^1, when the right choice is the one with the smallest mobility.

The presence of a small peak at the mobility of the dimer ion 1^1 and the mass of the monomer 0^1 is puzzling. This ion has gone through the DMA as the dimer and turned into the bare ion A^+ during its transit to the MS. This paradoxical observation, repeated at the mobility of 2^1 and the mass of 1^1, has been more generally confirmed and explained by subsequent studies as due to evaporation of neutral ion pairs [27,28]. We shall later see that a source of 0^1 and 1^1 ions is the decomposition of large unstable multiply charged ion covering a wide range of mobilities, which explains why the masses of 0^1 and 1^1 exhibit a quasi-continuum mobility spectrum clearly seen in Fig. 6 (left) as a long line extending to the right at $n/z = 0$ and 1.

4.4. Multiply charged ions

Fig. 6 shows a series of bands with positive slope, each corresponding to n^z clusters of variable n and fixed z. Most easily identified are those on the lower right, labeled in the right margin of the figure with their z values: 3, 5, 7. The complete $z = 2$ series is visible in Fig. 6a. It starts clearly at $n/z = 5 + (1/2)$ ($V = 3080$ V), but can be extended down to the 10^2 cluster by continuity. Like in the singly charged series, there are several possible assignments. The peaks associated to the original ions (no transition) are the ones most to the bottom right, with well-defined bands marked 3, 5, 7 on the right margin of the right image. Individual ions can be resolved in these bands well enough to ascertain their charge state up to $z = 10$, though the noise level is adequate to infer precise mobilities for a series of mass-selected peaks only up to $z = 6$. But the bands can be distinguished from each other past $z = 15$, providing mobility information without exact mass assignment (within the relatively narrow width of these bands) beyond $n \sim 300$ ($m \sim 130{,}000$ Da).

4.4.1. Peak assignment and charge loss transitions

In order to provide a systematic peak assignment, we have examined all the series of peaks of fixed z forming continuous lines in Fig. 6. Some, like the ones labeled 3, 5, 7 on the right of Fig. 6b can be easily discerned. The main peak voltages identified by this procedure are represented in Fig. 8 as a function of the cluster size n for charge states from $z = 1$ up to 8. One sees up to three $V^z(n)$ curves for most charge states z. Interestingly, many of these coincide to a first approximation with the $V^{z\pm1}(n)$ curves associated with the neighboring z values. One within each of these triplets of curves is evidently the genuine $V^z(n)$ relation, while the other two are due to a transition from an initial charge state z in the DMA measurement to a final charge state $z–p$ in the MS measurement. The data show that most of these transitions are associated, respectively, to loss of $(ABr)A^+$. As already noted, these transitions must take place downstream of the DMA, since otherwise the mobility peaks would not be narrow. The ions are therefore completely stable at atmospheric pressure. They are not purposely activated at the entry of the vacuum system leading to the MS (where our declustering voltage is only 1 V). Their instability is therefore almost surely due to RF heating in the ion guide. Accordingly, the peak voltage measured for these unstable ions corresponds to the precursor ion n^z selected on the DMA, while the mass measured corresponds to the product ion. Because these transitions preserve n or diminish it at most by one or two units (as we shall see shortly), the original $V(n)$ relation for the precursor ion n^z is preserved (or almost preserved) in the product ion, except that the label z inferred from the mass spectral data is reduced by one unit with respect to the value that would result in the absence of conversions. Let us focus, for instance, on

Table 2
Peak voltages for singly and doubly charged ions.

V (V)	1273	1956	2453	2865	3148	3556	2967	3129	3272	3424
m/z (Da)	355	789	1224	1658	2093	2528	2528	2745	2962	3180
n	0	1	2	3	4	5	10	11	12	13
z	1	1	1	1	1	1	2	2	2	2

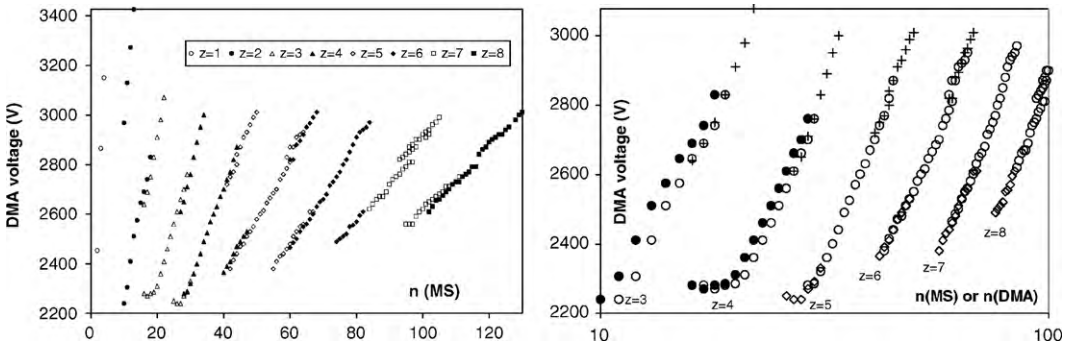

Fig. 8. Peak voltage of precursor ion versus cluster size n at charge states z from 1 to 9. Left: raw data with z and n based on the MS measurement, which may correspond to product ions of unstable clusters. Right: z is that of the precursor ion (z_{DMA}). (+) Symbols correspond to unreacted ions ($n_{MS} = n_{DMA}$); filled and open circles correspond to $z \rightarrow z-1$ products, plotted versus n_{MS} and n_{DMA}, respectively. Diamonds correspond to $z \rightarrow z-2$ products plotted versus n_{DMA}.

Table 3
Fragment loss for the $z_{MS} = z_{DMA} - 1$ or $z_{MS} = z_{DMA} - 2$ transitions observed.

z_{MS}	2	3	3	4	4	5	5	6	6	7	7	8
z_{DMA}	3	4	5	5	6	6	7[a]	7[a]	8[a]	8[a]	9[a]	9[a]
Fragment	1^1	1^1	$1^1 + 0^1$	1^1	2×1^1	1^1	2×1^1	1^1	2×1^1	1^1	2×1^1	1^1

[a] Based on indirect evidence (Fig. 9), since no mobility data are available at $z_{DMA} \geq 7$ for ions for which $z_{DMA} = z_{MS}$.

the three filled triangle data of Fig. 8 (left), all of which appear with four charges in the MS. Only the upper one corresponds really to $z = 4$. The other two correspond to substantially more mobile ions (smaller V at given n) that must have gone through the DMA at a higher charge state, presumably $z = 5$ and 6. The same can be seen with the white triangles associated to $z = 3$ in the MS. The upper one corresponds to precursor ions having gone through the DMA with $z = 3$, but the two lower more mobile data series have gone through the DMA with $z = 4$ and 5, and have lost one charge prior to mass measurement.

Let us now focus on the slight horizontal displacement so far ignored between the $V(n)$ curves corresponding to ions for which $z_{DMA} = z_{MS}$, and those for which one or two charges have been lost after DMA selection. One can see a systematic horizontal displacement by one or two n units for ions having undergone $z \rightarrow z-1$ or $z \rightarrow z-2$ transitions, respectively. The exception is for the clusters having passed from $z_{DMA} = 5$ to $z_{MS} = 3$, for which the reduction in n is by one unit only rather than two. This means that most charge loss events take place by ejection of a 1^1 ($ABrA^+$) fragment, with the exception noted where one of the two charge losses is associated to ejection of just A^+:

$$n^z \rightarrow (n-1)^{z-1} + 1^1 \quad (3b)$$

The minor fragment lost in each transition is shown in Table 3. This point is more strongly confirmed in Fig. 8 (right), where the various data sets are grouped according to z_{DMA}, and the horizontal variable used to plot the unfilled symbols is n_{DMA}, obtained from n_{MS} by adding the number of salt molecules ABr lost in the transition, as indicated in Table 3. The various types of ions plotted are distinguished by their different origins (+ for $z \rightarrow z$; ◯ for $z \rightarrow z-1$ and diamonds for $z \rightarrow z-2$). With this slight correction in the horizontal variable, the data for the three kinds of ions fall into a single curve. The figure includes also two data sets for $z \rightarrow z-1$ ions ($z_{DMA} = 3$ and 4), plotted versus n_{MS} (filled circles ●). The distance between open and filled circles is considerably larger than the typical scatter within open symbols, illustrating the fact that the DMA resolution is sufficient to clearly detect the loss of a single ion pair. Note in Fig. 8 (right) that we do not have $z \rightarrow z$ data for $z_{DMA} \geq 7$, so the evidence behind the claim that charge loss proceeds primarily by shedding the dimer ion 1^1 is in this case less direct (vide infra).

Additional direct evidence of the existence of many unstable ions that shed primarily the dimer cluster 1^1 can be seen also in Fig. 7 (left), showing that this ion appears at singular abundance over a wide range of mobilities. The same holds for the two other ions 0^1 and 2^1, but with a considerably smaller abundance.

4.4.2. Shape transitions

Two interesting peculiarities of our data are manifest in Fig. 8 (left). First, the mobility ceases suddenly to increase with decreasing cluster size for the lowest (most mobile) data for $z_{DMA} = 4$ and 5. Instead, it stays at an almost fixed value, or even decreases slightly. This singular behavior points to a shape transition from a relatively compact approximately spherical configuration to a more elongated structure. For *hard* spheres of radius R and charge z, the mobility is $Z \sim z/(R + R_g)^2$, where R_g is the hard sphere radius of the colliding gas molecule. Of course neither the clusters nor the gas molecules are hard spheres, but the notion is still useful to make qualitative shape inferences. The mass of that hypothetical sphere would be $m \sim R^3$. Accordingly, for spheres, $R \sim (z/Z)^{1/2} \sim m^{1/3} \sim (n+z)^{1/3}$. Therefore a plot of $(z/Z)^{1/2}$ versus $(n+z)^{1/3}$ should yield a single straight line for all n and z. Such a plot is shown in Fig. 9, displaying indeed the collapse into a unique approximately straight line, except for the anomalous horizontal high mobility data at the bottom of the curves for $z_{DMA} = 4$ and 5.

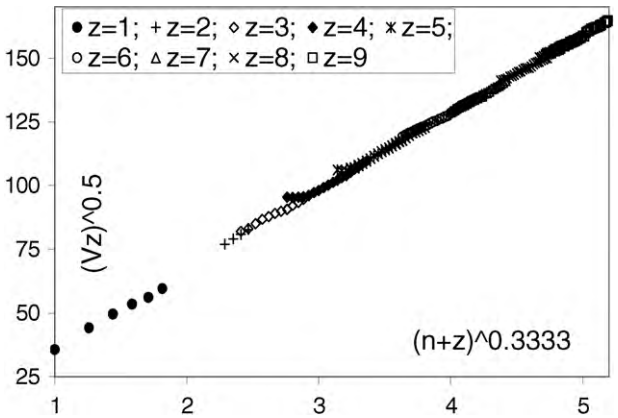

Fig. 9. Representation of the data of Fig. 8 in the form $(Vz_{DMA})^{1/2}$ ($V^{1/2}$) versus $(n_{DMA} + z_{DMA})^{1/3}$, showing an approximate collapse into a straight line for all z and n, as expected for nearly spherical clusters. Note the anomaly of the smallest clusters at charge states 4 and 5, revealing loss of a compact structure.

Another useful revelation of Fig. 9 is that the data are as continuous for charge states 1–6 (for which we have mobility measurements on the precursor ions confirming directly the loss of 1^1), as for charge states 7–9 (for which we do not). This provides strong evidence supporting the charge reduction path (3b) also for these higher charge states.

5. Conclusions

The DMA has demonstrated its potential to be coupled to several API–MS instruments to perform mobility selection upstream the mass spectrometer, with high transmission of the selected ion, and at resolving powers $R > 50$. Of particular practical interest is the ease with which a DMA can be coupled to many existing mass spectrometers without modifying the MS. This fact alone will help widen the number of laboratories with IMS–MS instrumentation. Use of a common round orifice at the DMA sample exit and the MS sample inlet limits DMA resolution below 50 at sampling flow rates as small as 0.5 L/min. However, in ion outlet channels transitioning from a slit at the DMA end to a circular orifice at the MS side, sample flows of several L/min can be accommodated with $R > 50$. The combination of the DMA with a TOF instrument of high resolution and wide mass range has revealed a number of interesting new features in multiply charged salt clusters. In particular, the fast (<100 μs) and mild ion transit through the DMA enables the isolation and study of unstable clusters that do not survive intact through the inlet system of the mass spectrometer, even when all MS lens voltages are kept at 1 V. The main transition observed in salt clusters of composition $(ABr)_n(A^+)_z$ is evaporation of one cation attached to a neutral ion pair: $(ABr)_n(A^+)_z \rightarrow (ABr)_{n-1}(A^+)_{z-1} + ABA^+$.

Acknowledgments

We are grateful to Mrs. Marta Hernández (CARTIF), Miriam Macía, Guillermo Vidal and Jordi Freixa (SEADM) for their help with many aspects of this development. The mechanical design includes contributions from Mr. Jerzy Kozlowski (AMPOL Tools Inc., West Haven, CT). We are also much indebted to Dr. Bruce A. Thomson of Sciex and Mr. Ikuo Konishi of Shimadzu Research Laboratory (Europe) Limited for many insights on the MS ends of the instrument. Also to Prof. Peter McMurry (U. Minnesota) for suggesting the tandem DMA method to measure transmission. This work has been fully financed by SEADM.

Appendix A. Resolution of a flat DMA with circular outlet orifice

Consider the simplest case of an incompressible flow where the fluid has a horizontal uniform velocity field $U = Ue_x$ along the x axis, to which is superposed a *sink* flow $qe_r/(2\pi r^2)$ associated to the fluid sampled by the orifice, written here in terms of the polar spherical coordinate r, and where q is the flow rate sampled from a half-plane (the lower half-plane below the lower electrode is outside the flow field). The *sink* is located on the surface of the lower electrode, and is taken for simplicity to be of negligibly small dimensions. Because the *sink* velocity field decays rapidly, as r^{-2}, it has no influence on the flow field slightly upstream, except for the fact that the orifice captures a semicircular piece of the fluid of radius:

$$R = \sqrt{\frac{2q}{\pi U}}, \tag{A1}$$

such that the flows q and $\pi R^2 U/2$ match exactly. The implication is that the flow sampled originates in a region of dimensions R, containing ions whose mobilities Z are previously separated in the two-dimensional field as:

$$\frac{Z}{Z_o} = 1 - \frac{y}{\Delta}, \tag{A2}$$

where y is the vertical height above the lower plate, Z_o is the mobility selected right at the bottom plate in the absence of suction, and Δ is the separation between the two parallel electrodes. Given the semicircular shape of the sample flow, each mobility within the spanned sampled range $Z/Z_o = 1 - R/\Delta$ is sampled with a probability proportional to $(1 - y^2/R^2)^{1/2}$:

$$p(Z) \sim \sqrt{1 - \left((1 - \frac{Z}{Z_o})\frac{\Delta}{R}\right)^2} \text{ for } 1 > \frac{Z}{Z_o} > 1 - \frac{R}{\Delta};$$

$$p(Z) = 0 \text{ outside that range.} \tag{A3–4}$$

FWHM for Z is therefore defined at the point where $(1 - y^2/R^2)^{1/2} = 1/2$, where:

$$\frac{y}{R} = \frac{\sqrt{3}}{2} \text{ and } \left(\frac{\Delta Z}{Z_o}\right)_{\text{FWHM}} = \frac{\sqrt{3}R}{2\Delta} \tag{A5}$$

Using now the definition (A1) of R we find:

$$\text{FWHM}^2 = \frac{3q}{2\pi U \Delta^2} = \frac{3W}{2\pi\Delta}\frac{q}{Q}. \tag{A6}$$

Except for the geometric factor of order unity $3W/(2\pi\Delta)$, FWHM scales as $(q/Q)^{1/2}$. This results therefore in a much larger resolution penalty than in a flat plate (or a cylindrical) DMA, where the symmetry of both sampling slits matches that of the DMA electrodes, and FWHM = q/Q [9].

In practice, q is fixed by the MS, and U is limited by the speed of sound. (A6) then shows the advantage of using relatively large Δ values. This consideration has led to the selection of $\Delta = 1$ cm in all prototypes interfaced to date to a MS. Then, at Mach number 0.5 ($U \sim 170$ m/s in room temperature air), and with $q = 0.5$ L/min, it is possible to achieve a resolution of 65. For many contemporary MS instruments sampling one or more L/min, it is preferable to shift to elongated outlet slits rather than increasing Δ further.

Note finally that the analysis just presented ignores effects occurring within a distance to the outlet of the order of its diameter. These may lead to non-negligible corrections, as may compressibility phenomena, also ignored here. In fact, the Senior Thesis of Juan Rus (unpublished) reported the discovery of three-dimensional effects turning into elliptical the ingested stream tube, which in the present approximation is circular. Interestingly, this effect did lead to resolving powers *higher* than predicted here, which were accounted for by including the finite size of the orifice in the analysis.

References

[1] R.W. Purves, R. Guevremont, S. Day, C.W. Pipich, M.S. Matyjaszczyk, Mass spectrometric characterization of a high-field asymmetric waveform ion mobility spectrometer, Rev. Sci. Instrum. 69 (1998) 4094–4104.
[2] A.A. Shvartsburg, K. Tang, R.D. Smith, FAIMS operation for realistic gas flow profile and asymmetric waveforms including electronic noise and ripple, J. Am. Soc. Mass Spectrom. 16 (2005) 1447–1455.
[3] P. Martínez-Lozano, J. Fernández de la Mora, Resolution improvements of a nano-DMA operating transonically, J. Aerosol Sci. 37 (2006) 500–512.
[4] H.A. Erikson, The change of mobility of the positive ions in air with age, Phys. Rev. 18 (1921) 100–101.
[5] H.F. Tammet, The aspiration method for the determination of atmospheric-ion spectra, Israel Program for Scientific Translations, Jerusalem, 1970 (original work in Russian from 1967).
[6] R.C. Flagan, History of electrical aerosol measurements, Aerosol Sci. Technol. 28 (1998) 301–380.
[7] J. Fernandez de la Mora, Diffusion broadening in converging differential mobility analyzers, J. Aerosol Sci. 33 (2002) 411–437.
[8] S.K. Friedlander, Smoke, Dust and Haze, Oxford University Press, 2000.
[9] E.O. Knutson, K.T. Whitby, Aerosol classification by electric mobility: apparatus, theory and applications, J. Aerosol Sci. 6 (1975) 443–451.

Please cite this article in press as: J. Rus, et al., Int. J. Mass Spectrom. (2010), doi:10.1016/j.ijms.2010.05.008

[10] J. Rosell, I.G. Loscertales, D. Bingham, J. Fernández de la Mora, Sizing nanoparticles and ions with a short differential mobility analyzer, J. Aerosol Sci. 27 (1996) 695–719.
[11] J.B. Fen, M. Mann, C.K. Meng, S.F. Wong, C.M. Whitehouse, Electrospray ionization for mass spectrometry of large biomolecules, Science 246 (1989) 64–71.
[12] J. Fernández de la Mora, L. de Juan, T. Eichler, J. Rosell, Differential mobility analysis of molecular ions and nanometer particles, Trends Anal. Chem. 17 (1998) 328–339.
[13] J. Fernández de la Mora, B.A. Thomson, M. Gamero-Castaño, Tandem mobility mass spectrometry study of electrosprayed $Heptyl_4N^+Br^-$ clusters, J. Am. Soc. Mass Spectrom. 16 (2005) 717–732.
[14] S. Ude, J. Fernandez de la Mora, B.A. Thomson, Charge-induced unfolding of multiply charged polyethylene glycol ions, J. Am. Chem. Soc. 126 (2004) 12184–12190.
[15] J. Fernández de la Mora, L. de Juan, T. Eichler, J. Rosell, Method and apparatus for separating ions in a gas for mass spectrometry, US Patent 5,869,831 (9.02.99).
[16] S. Ude, Properties and measurement of nanometer particles in the gas phase, Ph.D. Thesis, Yale University, 2004.
[17] J. Fernández de la Mora, S. Ude, B.A. Thomson, The potential of differential mobility analysis coupled to mass spectrometry for the study of very large singly and multiply charged proteins and protein complexes in the gas phase, Biotechnol. J. 1 (2006) 988–997.
[18] J. Fernández de la Mora, M.J. Labowsky, J. Schmitt, W. Neilson, Method and apparatus to increase the resolution and widen the range of differential mobility analyzers (DMAs), US Patent, 6,787,763 (7.09.04).
[19] J. Rus, J. Fernandez de la Mora, Resolution improvement in the coupling of planar differential mobility analyzers with mass spectrometers or other analyzers and detectors, US Patent application publication 20,080,251,714 (16.10.08).
[20] J. Rus, F. Estévez, J. Fernández de la Mora, A planar DMA coupled to a MS for tandem IMS–MS separation at high transmission, with IMS resolution approaching 100, in: Poster 105, ASMS Conference, Indianapolis, 3–7 June, 2007.
[21] H. Javaheri, Y. Le Blanc, B.A. Thomson1, J. Fernandez de la Mora, J. Rus, J.A. Sillero-Sepúlveda, Analytical characteristic of a differential mobility analyzer coupled to a triple quadrupole system (DMA–MSMS), in: Poster 061, Annual ASMS Conference, Denver, Colorado, 1–6 June, 2008.
[22] J. Rus, D. Moro, J.A. Sillero, J. Freixa, J. Fernández de la Mora, A high flow rate DMA with high transmission and resolution designed for new API instruments, in: Poster 042, Annual ASMS Conference, Denver, Colorado, 1–6 June, 2008.
[23] J. Zhao, F.L. Eisele, M. Titcombe, C. Kuang, P.H. McMurry, Chemical ionization mass spectrometric measurements of atmospheric neutral clusters using the cluster-CIMS, J. Geophys. Res., ~~in press~~.
[24] S. Ude, J. Fernández de la Mora, Molecular monodisperse mobility and mass standards from electrosprays of tetra-alkyl ammonium halides, J. Aerosol Sci. 36 (2005) 1224–1237.
[25] C.K. Meng, J.B. Fenn, Formation of charged clusters during electrospray ionization of organic solute species, Org. Mass Spectrom. 26 (1991) 542–549.
[26] S. Myung, M. Fioroni, R.R. Julian, S.L. Koeniger, M.-H. Baik, D.E. Clemmer, Chirally directed formation of nanometer-scale proline clusters, J. Am. Chem. Soc. 128 (2006) 10833–10839.
[27] C.J. Hogan Jr., J. Fernandez de la Mora, Ion-pair evaporation from ionic liquid clusters, J. Am. Soc. Mass Spectr., ~~submitted for publication~~.
[28] C.J. Hogan Jr., J. Fernández de la Mora, Tandem ion mobility-mass spectrometry (IMS–MS) study of ion evaporation from ionic liquid-acetonitrile nanodrops, Phys. Chem. Chem. Phys. 11 (2009) 8079–8090.

Please cite this article in press as: J. Rus, et al., Int. J. Mass Spectrom. (2010), doi:10.1016/j.ijms.2010.05.008